Journal of Alloys and Compounds 648 (2015) 1–6

Contents lists available at ScienceDirect

Journal of Alloys and Compounds

journal homepage: http://www.elsevier.com/locate/jalcom

The influence of replacing the pnicogens As by Sb on the optical properties of the Zintl phases $Ba_2Cd_2Pn_3$ (Pn = As and Sb)

A.H. Reshak [a, b, *]

[a] New Technologies – Research Centre, University of West Bohemia, Univerzitni 8, 306 14 Pilsen, Czech Republic
[b] Center of Excellence Geopolymer and Green Technology, School of Material Engineering, University Malaysia Perlis, 01007 Kangar, Perlis, Malaysia

ARTICLE INFO

Article history:
Received 18 May 2015
Received in revised form
24 June 2015
Accepted 25 June 2015
Available online 30 June 2015

Keywords:
Optical properties
Pnicogens
Zintl phases
mBJ

ABSTRACT

We explored the influence of changing the pnicogens by substituting As by Sb on the optical properties of $Ba_2Cd_2Pn_3$ (Pn = As and Sb). Calculation show that there exists subtle difference in the electronic structures when we substitute As by Sb, which lead to significant influence on the optical properties, taking into account the size and the electro-negativity differences between As and Sb atoms. The full potential method within the recently modified Becke-Johnson potential explore that the $Ba_2Cd_2Pn_3$ (Pn = As and Sb) compounds are narrow band gap semiconductors of about 0.49 and 0.32 eV. The optical properties explore that these material have negative uniaxial anisotropy, negative birefringence and considerable anisotropy between the optical components in the polarization directions [100], [010] and [001] with respect to the crystal axis. Furthermore, the optical properties confirm that $Ba_2Cd_2Sb_3$ possess a band gap which is smaller than that of $Ba_2Cd_2As_3$. The optical properties helps to get deep insight into the electronic structure.

1. Introduction

The intermetallic compounds are formed by two or more metals which represent very important group of chemical compounds [1]. Intermetallic compounds are promising candidates for several applications for instance as superconductors [2], refractory high-strength super alloys [3] magnetic compounds [4] and metallic glasses for possible applications in fuels cells [3]. The importance of the intermetallic compounds has been proven by several discoveries of polar intermetallics and Zintl phases which display complex combinations of structural, electronic, magnetic, thermal and transport properties [5–10]. Edward Zintl pioneered a new class of intermetallic compounds called Zintl phases, which constitute a large class of inorganic materials with very various crystal structures [11–14]. Since the discovery of the Zintal phases a large number of new Zintal compounds have been synthesized, and their structural and electronic characterizations have given tremendous information about their structure property relationship [15–22]. It has been found that in Zintl phase the nature of the chemical bonding can be understood by assuming a complete transfer of electrons from the more electropositive metal to the more electronegative element [23,24]. Due to their complex structure, Zintl phases have been classified as promising candidates for thermoelectric applications. Their electronic structure enable favorable thermal conductivity and the optimal charge transport properties [25,26]. Among the new promising Zintl phases are $Ba_2Cd_2As_3$ and $Ba_2Cd_2Sb_3$. Recently, these two compounds have been synthesized and characterized by Saparov et al. [18]. They reported that these compounds crystallize in a novel monoclinic structure with the space group C2/m featuring polyanionic layers made of Cd Pn_4 tetrahedra (Pn = As or Sb) and homoatomic Pn–Pn bonds. We should emphasize that the cationic subsystem and phonon interactions may play principal role to modify the obtained optical spectra [27].

Due to dearth information regarding the electronic structure and the optical properties of $Ba_2Cd_2Pn_3$ (Pn = As and Sb) compounds and due to the unique structure of these compounds [21,30,31], as well as the underestimation of the band gap of $Ba_2Cd_2Sb_3$ by the TB-LMTO-ASA calculation. Therefore, we thought it is worthwhile to perform comprehensive theoretical calculation based on the density fictional theory within the recently modified Becke-Johnson potential (*mBJ*) [28] to investigate the electronic band structure, density of states, electronic charge density distribution and the optical properties. The optical properties can give

* New Technologies – Research Centre, University of West Bohemia, Univerzitni 8, 306 14 Pilsen, Czech Republic.
E-mail address: maalidph@yahoo.co.uk.

http://dx.doi.org/10.1016/j.jallcom.2015.06.207
0925-8388/

deep insight into the electronic structure. It has been proven that the first-principles calculation is a strong and useful tool to predict the crystal structure and its properties related to the electron configuration of a material before its synthesis [29–32].

2. Details of calculation (from structure)

$Ba_2Cd_2Pn_3$ (Pn = As or Sb) crystallizes in Zintl phases with monoclinic space group $C2/m$, it contains two Ba, two Cd and three As or Sb atoms situated in special positions (symmetry independent) [18]. The atomic arrangement of these atoms make the structure of $Ba_2Cd_2Pn_3$ unique, it has two dimensional layers [18,33,34]. Based on the reported x-ray diffraction data (XRD) of $Ba_2Cd_2Pn_3$ (Pn = As or Sb) [18], a comprehensive theoretical calculation within density functional theory (DFT) was performed. The full potential linear augmented plane wave (*FPLAPW + lo*) method as embodied in the *WIEN* 2*k* code [35] within generalized gradient approximation (*PBE−GGA*) [36] were used to perform the geometrical relaxation. The resulting relaxed geometries were used to calculate the electronic structure and hence the associated properties using the recently modified Becke-Johnson potential (*mBJ*) [28]. The relaxed crystal structures of $Ba_2Cd_2Pn_3$ (Pn = As or Sb) along with the asymmetric unit were presented in Fig. 1. The unit cell was divided into two regions, the spherical harmonic expansion was used inside the non-overlapping spheres of muffin-tin radius (R_{MT}) and the plane wave basis set was chosen in the interstitial region (*IR*) of the unit cell. The R_{MT} for Ba, Cd, As and Sb were chosen in such a way that the spheres did not overlap, these values are 2.5 a.u for Ba, Cd, Sb and 2.3 a.u. for As. In order to get the total energy convergence, the basis functions in the *IR* were expanded up to $R_{MT} \times K_{max} = 7.0$ and inside the atomic spheres for the wave function. The maximum value of $\boldsymbol{l}$ was taken as $\boldsymbol{l}_{max} = 10$, while the charge density is Fourier expanded up to $G_{max} = 12\ (a.u)^{-1}$. Self-consistency is obtained using 300 $\vec{k}$ points in the irreducible Brillouin zone (*IBZ*). The self-consistent calculations are converged since the total energy of the system is stable within 0.00001 Ry. The electronic band structures calculation are performed within 1500 $\vec{k}$ points in the *IBZ*.

The monoclinic symmetry allows three non-zero components of the second-order optical dielectric tensor corresponding to the electric field $\vec{E}$ being directed along **a**, **b**, and **c**-crystallographic axes. We identify these with the *x*, *y* and *z* Cartesian directions. The imaginary part of the three principal complex tensor components completely defines the linear optical susceptibilities. These are $\varepsilon_2^{xx}(\omega)$, $\varepsilon_2^{yy}(\omega)$ and $\varepsilon_2^{zz}(\omega)$ which originates from inter-band transitions between valence and conduction bands. The imaginary parts can be calculated using the following expression [37]:

$$\varepsilon_2^{ij}(\omega) = \frac{8\pi^2\hbar^2e^2}{m^2V}\sum_k\sum_{cv}(f_c - f_v)\frac{p_{cv}^i(k)p_{vc}^j(k)}{E_{vc}^2}\delta[E_c(k) - E_v(k) - \hbar\omega] \tag{1}$$

where m, e and $\hbar$ are the electron mass, charge and Planck's constant, respectively. f_c and f_v represent the Fermi distributions of the conduction and valence bands, respectively. The term $p_{cv}^i(k)$ denotes the momentum matrix element transition from the energy level c of the conduction band to the level v of the valence band at certain **k**-point in the BZ and V is the unit cell volume. The real part $\varepsilon_1(\omega)$ of the dielectric function can be evaluated from $\varepsilon_2(\omega)$ with the aid of Kramer-Kronig relationship [39].

$$\varepsilon_1(\omega) = 1 + \frac{2}{\pi}P\int_0^\infty \frac{\omega'\varepsilon_2(\omega')}{\omega'^2 - \omega^2}d\omega' \tag{2}$$

where P implies the principal value of the integral.

3. Results and discussion

3.1. Salient features of the electronic band structures (from thermo)

Since the electronic band structure helps to understand the mechanism of the optical transitions therefore, we have calculated the electronic band structure of $Ba_2Cd_2As_3$ and $Ba_2Cd_2Sb_3$ compounds within *PBE−GGA* and the recently modified Becke-Johnson potential as shown in Figs. S1 and S2(a), (b) as a supplementary materials. It is well known that the area in vicinity of Fermi level (E_F) play an important rule for the carrier's transportation therefore, as prototype we illustrated the electronic band structure of $Ba_2Cd_2As_3$ along with the optical transitions depicted on a generic band structure using *mBJ* as shown in Fig. 1. It is clear that the upper valence band (Fig. 1) shows flat **k**-dispersion. This reflects the low mobility of the holes. Whereas the lower conduction band exhibit highest **k**-dispersion which imply lowest effect masses and hence the highest mobility for the electrons. The calculated electron effective mass (m_e^*) and effective mass ratio (m_e^*/m_e) of $Ba_2Cd_2As_3$ are 0.0617×10^{-31} and 0.0067, while for $Ba_2Cd_2Sb_3$ are 0.0539×10^{-31} and 0.0059. It has been found that the $Ba_2Cd_2As_3$ compound possess narrow direct energy gap of about 0.49 eV while the $Ba_2Cd_2Sb_3$ compound exhibit narrower indirect energy gap of about 0.32 eV. Therefore, the electronic structures of these compounds allow the optimal charge transport properties. It is well known that the nature of the chemical bonding in $Ba_2Cd_2As_3$ and $Ba_2Cd_2Sb_3$ compounds can be understood by assuming a complete transfer of electrons from the more electropositive metal (here Ba and Cd) to the more electronegative element (As and Sb). According to Pauling scale the electronegativity of As and Sb are 2.18 and 2.05, whereas the electronegativity of Ba and Cd are 0.89 and 1.69 thus they possess high electropositivity of about 3.11 and 2.31. Therefore, they are similar to the typical semiconductors. Due to the atomic radii differences, substituting As by Sb lead to increase the bond distance which influence the degree of covalency between Ba-Pn (Pn = As or Sb) [18]. Covalent bonding is more favorable for the transport of the carriers than ionic one [38].

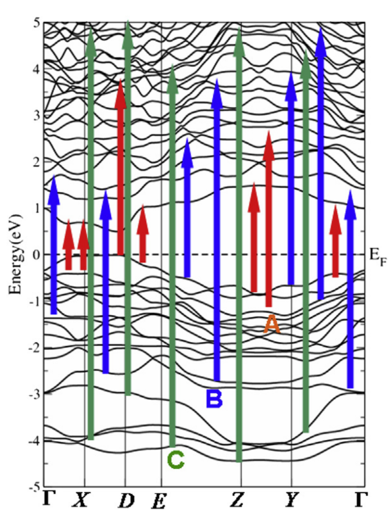

Fig. 1. The optical transitions depicted on a generic band structure of the $Ba_2Cd_2As_3$ as prototype.

3.2. Optical response

The optical properties can provide detailed information about the electronic structure of the materials. The optical properties of solids are a major topic, both in basic research as well as for industrial applications. While for the former the origin and nature of different excitation processes is of fundamental interest, the latter can make use of them in many optoelectronic devices. Deep insight into the electronic structure of $Ba_2Cd_2Pn_3$ (Pn = As or Sb) can be obtained from the investigated optical properties of these materials. Therefore, we have calculated the imaginary and real parts of the frequency dependent optical dielectric functions. The calculations of the frequency-dependent dielectric function involve the energy eigenvalues and electron wavefunctions. The optical components are determined by inter-band transitions from valence-into conduction-bands. According to the dipolar selection rule only transitions changing the angular momentum quantum number l by unity ($\Delta = \pm 1$) are allowed.

The linear response of the system to electromagnetic radiation can be described by means of the dielectric function $\varepsilon(\omega)$ which is related to the interaction of photons with electrons. Two kinds of contributions to $\varepsilon(\omega)$ are usually distinguished, namely intra-band and inter-band electronic excitations. Intra-band transitions are not present in semiconductors, as they are present only for metals and semi-metals. The dispersion of the imaginary part of the dielectric function $\varepsilon_2(\omega)$ can be calculated from the momentum matrix elements between the occupied and unoccupied wavefunctions, giving rise to the selection rules.

In Fig. 2(a) and (b) we illustrated the imaginary part of the optical components $\varepsilon_2^{xx}(\omega)$, $\varepsilon_2^{yy}(\omega)$ and $\varepsilon_2^{zz}(\omega)$ along with the real parts $\varepsilon_1^{xx}(\omega)$, $\varepsilon_1^{yy}(\omega)$ and $\varepsilon_1^{zz}(\omega)$. It is clear that $\varepsilon_2(\omega)$ of $Ba_2Cd_2As_3$ and $Ba_2Cd_2Sb_3$ exhibit only one main structure located around 4.0 eV. Substituting As by Sb cause significant influence in the electronic structure and hence the optical properties, as it is clear that the main structure of $\varepsilon_2(\omega)$ in $Ba_2Cd_2Sb_3$ shift towards lower energies by around 0.17 eV with increasing the peak heights. Which confirms our previous observation that a band gap reduction occurs when we move from As to Sb, in concordance with the calculated electronic band structure and the density of states. The calculated band structure and the partial density of states helps to analyze the origin of the observed structures in $\varepsilon_2(\omega)$.

The optical transitions of the observed structures in $\varepsilon_2(\omega)$ are labeled according to the spectral peak positions in Fig. 2(a) and (b). As prototype we illustrated the optical transitions depicted on a generic band structure of the $Ba_2Cd_2As_3$ (Fig. 1). For simplicity, we have labeled the transitions in Figs. 1 and 2(a, b), as A, B, and C. The transitions (A) are responsible for the structures for $\varepsilon_2^{xx}(\omega)$, $\varepsilon_2^{yy}(\omega)$ and$\varepsilon_2^{zz}(\omega)$ in the spectral range 0.0–5.0 eV; the transitions (B) 5.0–10.0 eV, and the transitions (C) 10.0–14.0 eV. It has been found that they are due to the inter-band transitions between Cd-s/p, As/Sb-p bands to Cd-p, Ba-s/d and As/Sb-p/d bands according to the optical selection rules.

The vanishing frequency value of the dielectric function defines the static electronic dielectric constant $\varepsilon_1^{xx}(0)$, $\varepsilon_1^{yy}(0)$ and $\varepsilon_1^{zz}(0)$. The uniaxial anisotropy $\delta\varepsilon = [(\varepsilon_0^{II} - \varepsilon_0^{\perp})/\varepsilon_0^{tot}]$ can be obtained from the static electronic dielectric constant. It has been found that these materials exhibit negative uniaxial anisotropy. These values are listed in Table 1. The real part as shown in Fig. 2(a) and (b) confirming that moving from As to Sb cause a band gap reduction, this could be explained on the basis of the Penn model [40]. Penn proposed a relation between $\varepsilon(0)$ and E_g, $\varepsilon(0) \approx 1 + (\hbar\omega_P/E_g)^2$. E_g is some kind of averaged energy gap which could be related to the real energy gap. Thus, the larger $\varepsilon_1(0)$ value is corresponding to the small energy gap. This is an another evidence that $Ba_2Cd_2Sb_3$ possess a gap which confute the previous finding by TB-LMTO-ASA [18]. Also it confirm that $Ba_2Cd_2Sb_3$ exhibit a smaller energy than that of $Ba_2Cd_2As_3$.

There are other important features in the optical spectrum, such as plasmon oscillations, which are associated with inter-band transitions. The plasmon maximum is usually the most intense feature in the optical spectrum which occurs at energy where $\varepsilon_1(\omega)$

Table 1
The calculated energy band gap in comparison with the experimental value, $\varepsilon_1^{xx}(0)$, $\varepsilon_1^{yy}(0)$, $\varepsilon_1^{zz}(0)$, $\delta\varepsilon$, ω_p^{xx}, ω_p^{yy}, ω_p^{zz}, $n^{xx}(0)$, $n^{yy}(0)$, $n^{zz}(0)$ and $\Delta n(0)$ for $Ba_2Cd_2As_3$ and $Ba_2Cd_2Sb_3$ using *PBE−GGA* and *mBJ*.

	$Ba_2Cd_2As_3$		$Ba_2Cd_2Sb_3$	
	PBE−GGA	*mBJ*	*PBE−GGA*	*mBJ*
Eg (eV)	0.103	0.49	0.029	0.32
$\varepsilon_1^{xx}(0)$	13.78	10.06	16.66	12.13
$\varepsilon_1^{yy}(0)$	15.32	11.30	17.25	13.16
$\varepsilon_1^{zz}(0)$	17.54	10.75	18.04	12.96
$\delta\varepsilon$	−0.17	−0.09	−0.05	−0.07
ω_p^{xx}	4.14	4.44	3.57	3.79
ω_p^{yy}	3.82	4.14	3.22	3.60
ω_p^{zz}	3.79	4.09	3.19	3.49
$n^{xx}(0)$	3.71	3.17	4.08	3.48
$n^{yy}(0)$	3.91	3.36	4.15	3.62
$n^{zz}(0)$	4.19	3.27	4.80	3.60
$\Delta n(0)$	−0.38	−0.14	−0.68	−0.13

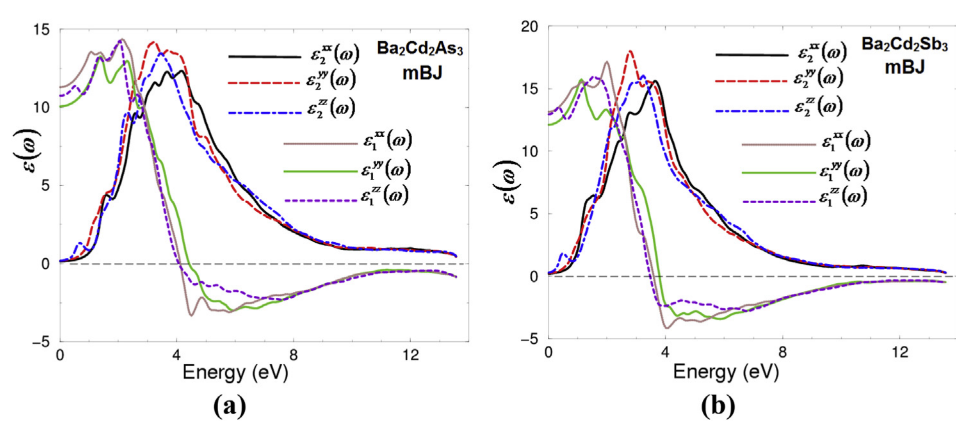

Fig. 2. (a) Calculated $\varepsilon_2^{xx}(\omega)$,$\varepsilon_2^{yy}(\omega)$ and $\varepsilon_2^{zz}(\omega)$ along with Calculated $\varepsilon_1^{xx}(\omega)$, $\varepsilon_1^{yy}(\omega)$ and $\varepsilon_1^{zz}(\omega)$ for $Ba_2Cd_2As_3$; (b) Calculated $\varepsilon_2^{xx}(\omega)$,$\varepsilon_2^{yy}(\omega)$ and $\varepsilon_2^{zz}(\omega)$ along with Calculated $\varepsilon_1^{xx}(\omega)$, $\varepsilon_1^{yy}(\omega)$ and $\varepsilon_1^{zz}(\omega)$ for $Ba_2Cd_2Sb_3$.

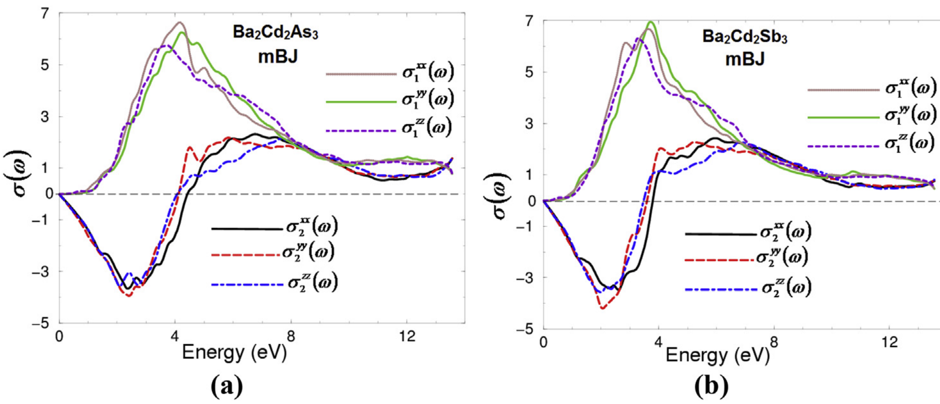

Fig. 3. (a) Calculated $\sigma_2^{xx}(\omega)$,$\sigma_2^{yy}(\omega)$ and $\sigma_2^{zz}(\omega)$ along with Calculated $\sigma_1^{xx}(\omega)$, $\sigma_1^{yy}(\omega)$ and $\sigma_1^{zz}(\omega)$ for $Ba_2Cd_2As_3$; (b) Calculated $\sigma_2^{xx}(\omega)$,$\sigma_2^{yy}(\omega)$ and $\sigma_2^{zz}(\omega)$ along with Calculated $\sigma_1^{xx}(\omega)$, $\sigma_1^{yy}(\omega)$ and $\sigma_1^{zz}(\omega)$ for $Ba_2Cd_2Sb_3$.

crosses zero, it is associated with the existence of plasma oscillations. The values of ω_p^{xx}, ω_p^{yy} and ω_p^{zz} for $Ba_2Cd_2As_3$ and $Ba_2Cd_2Sb_3$ compounds are listed in Table 1.

Using the existing information on the calculated $\varepsilon_2(\omega)$ and $\varepsilon_1(\omega)$ we can derive other optical properties. The imaginary and real parts of the optical conductivity as shown in Fig. 3(a) and (b) are directly related to the complex dielectric function which can be drive using the expression $\varepsilon(\omega) = \varepsilon_1(\omega) + i\varepsilon_2(\omega) = 1 + 4\pi i\sigma(\omega)/\omega$. The imaginary part $\sigma_2^{xx}(\omega)$, $\sigma_2^{yy}(\omega)$ and $\sigma_2^{zz}(\omega)$ between 0.0 and the values of ω_p^{xx} , ω_p^{yy} and ω_p^{zz} exhibit overturned features of $\varepsilon_2^{xx}(\omega)$, $\varepsilon_2^{yy}(\omega)$ and $\varepsilon_2^{zz}(\omega)$, whereas the real parts $\sigma_1^{xx}(\omega)$, $\sigma_1^{yy}(\omega)$ and $\sigma_1^{zz}(\omega)$ show similar features to that of $\varepsilon_2^{xx}(\omega)$, $\varepsilon_2^{yy}(\omega)$ and $\varepsilon_2^{zz}(\omega)$ with shift whole spectral structures towards higher energies by around 0.9 and 0.6 eV for $Ba_2Cd_2As_3$ and $Ba_2Cd_2Sb_3$. The optical reflectivity of $Ba_2Cd_2As_3$ and $Ba_2Cd_2Sb_3$ compounds as shown in Fig. 4(a) and (b) exhibit that the first reflectivity maximum occurs between 4.0 and 4.4 eV for $Ba_2Cd_2As_3$ while it is between 3.4 and 3.8 for $Ba_2Cd_2Sb_3$. These are the values of the plasma resonance which confirm the occurrence of a collective plasmon resonance in concordance with our observation in Figs. 2 and 3(a, b). All optical properties exhibit a lossless region around 12.0 eV and considerable anisotropy between the three components along the polarization directions [100], [101] and [001] in the observed energy interval.

Fig. 5(a and b) illustrated the calculated refractive indices for $Ba_2Cd_2Pn_3$ (Pn = As or Sb), it can be seen that $n^{xx}(0)$, $n^{yy}(0)$ and $n^{zz}(0)$ at zero frequency show the static refractive index. They increase beyond the zero frequency limits and reached to their maximum values. Beyond the maximum value they start to decrease and with few oscillations they go beyond unity. In this region (n < 1) the phase velocity of the photons increases to universal constant (C). However the group velocity always less than the C, therefore the relativity relations not effected [41]. The peaks in the spectra shift towards lower energy when we substitute As by Sb. The variation is in accordance to the decrease in the band gaps. The calculated values of zero frequency refractive indices are given in Table 1. It suggests that the refractive index at zero frequency is inversely related to the band gap ($n = \sqrt{\varepsilon}$).

The birefringence can be calculated from the linear response functions from which the anisotropy of the index of refraction is determined. The birefringence is the difference between the extraordinary and ordinary refraction indices, $\Delta n(\omega) = n_e(\omega) - n_o(\omega)$, where $n_o(\omega)$ is the index of refraction for an electric field oriented along the c-axis and $n_e(\omega)$ is the index of refraction for an electric field perpendicular to the c-axis. Fig. 5(c) shows the birefringence $\Delta n(\omega)$ dispersion of $Ba_2Cd_2Pn_3$ (Pn = As or Sb). It is clear that the birefringence is important only in the non-absorbing spectral range, which is below the energy gap. We find that $Ba_2Cd_2Pn_3$ (Pn = As or Sb) possesses a negative birefringence at zero energy as shown in Table 1.

4. Conclusions

As starting point of the current calculation the reported x-ray diffraction data (XRD) of $Ba_2Cd_2Pn_3$ (Pn = As or Sb) was used to perform a comprehensive theoretical calculation. The full

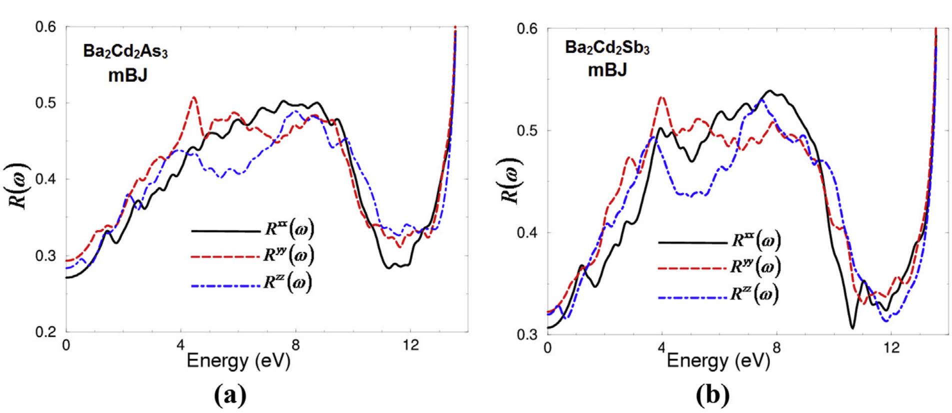

Fig. 4. (a) Calculated $R^{xx}(\omega)$, $R^{yy}(\omega)$, and $R^{zz}(\omega)$ for $Ba_2Cd_2As_3$; (b) Calculated $R^{xx}(\omega)$, $R^{yy}(\omega)$, and $R^{zz}(\omega)$ for $Ba_2Cd_2Sb_3$.

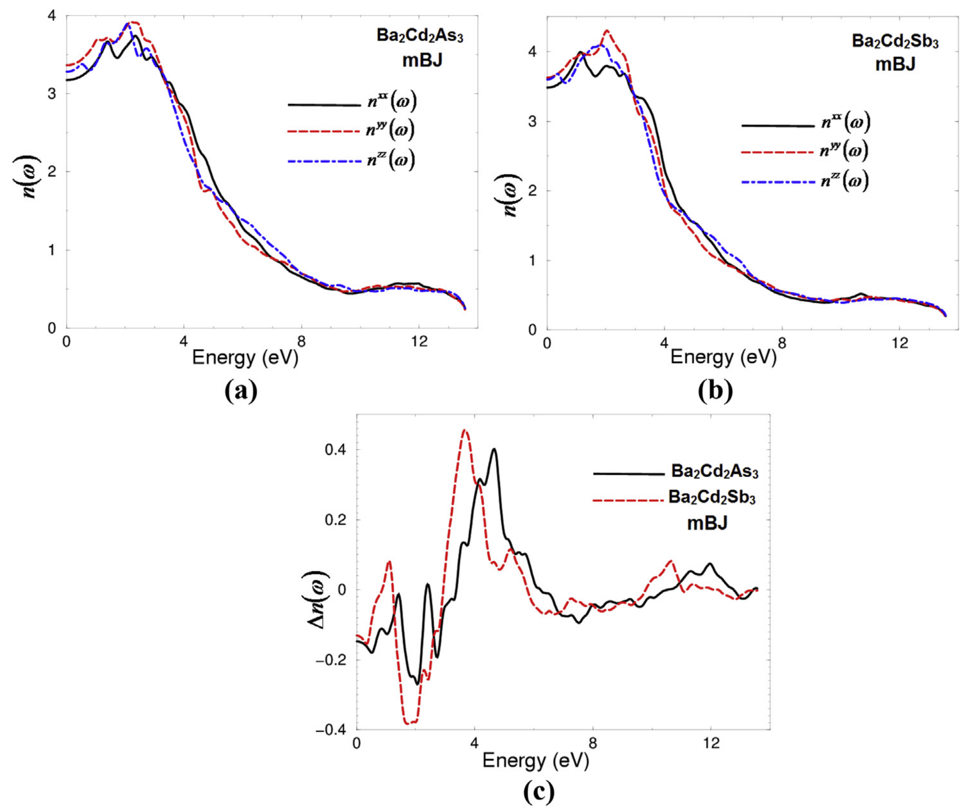

Fig. 5. (a) Calculated $n^{xx}(\omega)$, $n^{yy}(\omega)$, and $n^{zz}(\omega)$ for $Ba_2Cd_2As_3$; (b) Calculated $n^{xx}(\omega)$, $n^{yy}(\omega)$, and $n^{zz}(\omega)$ for $Ba_2Cd_2Sb_3$; (c) Calculated $\Delta n(\omega)$ for $Ba_2Cd_2As_3$ and for $Ba_2Cd_2Sb_3$.

potential linear augmented plane wave (*FPLAPW* + *lo*) method within generalized gradient approximation (*PBE*−*GGA*) were used to perform the geometrical relaxation. Both of *PBE*−*GGA* and the recently modified Becke-Johnson potential explore that the $Ba_2Cd_2Pn_3$ (Pn = As and Sb) compounds are narrow band gap semiconductors with subtle difference in band desperations of the two compounds. These differences cause significant influence on the optical transitions of these materials, taking into account the size and the electro-negativity differences between As and Sb atoms. To get deep insight into the electronic structure, the optical properties were calculated and analyzed in details. The optical properties exhibit that the $Ba_2Cd_2Pn_3$ (Pn = As or Sb) compounds possess negative birefringence, negative uniaxial anisotropy and considerable anisotropy between the optical components in the [100], [101] and [001] polarization directions. In concordance with our previous observation from the electronic band structure and the density of state, the optical properties exhibit that $Ba_2Cd_2Sb_3$ possess an energy gap which is smaller than that of $Ba_2Cd_2As_3$. The optical properties confirm the existence of the lossless region.

Acknowledgments

The result was developed within the CENTEM project, reg. no. CZ.1.05/2.1.00/03.0088, cofunded by the ERDF as part of the Ministry of Education, Youth and Sports OP RDI programme and, in the follow-up sustainability stage, supported through CENTEM PLUS (LO1402) by financial means from the Ministry of Education, Youth and Sports under the "National Sustainability Programme I. Computational resources were provided by MetaCentrum (LM2010005) and CERIT-SC (CZ.1.05/3.2.00/08.0144) infrastr uctures.

Appendix A. Supplementary data

Supplementary data related to this article can be found at http://dx.doi.org/10.1016/j.jallcom.2015.06.207.

References

[1] P. Villars, L.D. Calvert, Pearsons Handbook of Crystallographic Data for Intermetallic Compounds, second ed., ASM International, Materials Park, OH, 1991. Desk Edition, 1997.
[2] C.T. Sims, N.S. Stoloff, W.C. Hagel, Superalloys II, Wiley, New York, 1987.
[3] J.F. Herbst, in: G.J. Long, F. Grandjean (Eds.), Supermagnets, 1991.
[4] H. Hillman, in: S. Foner, B. Schwartz (Eds.), Superconductor Materials Science-metallurgy, Fabrication and Applications, 1981, p. 275. New York.
[5] R.B. Schwartz, in: J.H. Westbrook, R.L. Fleischer (Eds.), Intermetallic Compouds, Vol. 3, Wiley, New York, 2002, p. 681.
[6] J. Nagamatsu, N. Nakagawa, T. Muranaka, Y. Zenitani, J. Akimitsu, Nature 410 (2001) 6824.
[7] J.Y. Chan, S.M. Kauzlarich, P. Klavins, R.N. Shelton, D.J. Webb, Chem. Mater. 9 (1997) 3132.
[8] A.M. Campbell, Science 292 (2001) 65.
[9] D.-Y. Chung, T. Hogan, P. Brazis, M. Rocci-Lane, C. Kannerwurf, M. Bastea, C. Uher, M. Kanatzidis, Science 287 (2000) 1024.
[10] H. Kawaji, H. Horie, S. Yamanaka, M. Ishikawa, Phys. Rev. Lett. 74 (1995) 1427.
[11] E. Zintl, Angew. Chem. 52 (1939) 1.
[12] E. Zintl, G. Brouer, Z. Phys. Chem. 820 (1933) 245.
[13] E. Zintl, W. Dullenkopf, Z. Phys. Chem. B16 (1932) 183.
[14] E. Zintl, G. Woltersdorf, Z. Electrochem. 41 (1935) 876.
[15] J.D. Corbett, in: S.M. Kaurlarich (Ed.), Chemistry, Structure, and Bonding of Zintl Phases and Ions, VCH, New York, 1996, p. 139.
[16] J.D. Corbett, Structure & Bonding, vol. 87, 1997, p. 157.
[17] I.D. Corbett, Angew. Chem. Int. Ed. 39 (2000a) 670.
[18] Bayrammurad Saparov, Hua He, Xiaohang Zhang, Richard Greeneb, Svilen Bobev, Dalton Trans. 39 (2010) 1063–1070.
[19] G.J. Miller, in: S.M. Kauzlarich (Ed.), Chemistry, Structure, and Bonding of Zintl Phases and Ions, VCH, New York, 1996, p. 1.
[20] B. Eisenmann, G. Cordier, in: Chemirtry, Structure and Bonding of Zintl Phases and Ions (4. S. M. Kauzlarich), VCH Publishers, Inc., New York, NY, 1996, p. 61.
[21] W. van der Lugt, in: S.M. Kauzlarich (Ed.), Chemistry, Shucture, AndBonding of Zintl Phases and Ions, VCH, New York, 1996, p. 183.

[22] C. Belin, M. Tillard-Charbonnel, Prog. Solid St. Chem. 22 (1993) 59.
[23] E. Zintl, Angew. Chem. 52 (1939) 1. Chemistry, Structure, and Bonding of Zintl Phases and Ions, ed. S. M. Kauzlarich, VCH Publishers, New York, 1996.
[24] R. Nesper, Prog. Solid State Chem. 20 (1990) 1.
[25] G.J. Snyder, E.S. Toberer, Nat. Mater. 7 (2008) 105.
[26] S.M. Kauzlarich, S.R. Brown, G.J. Snyder, Dalton Trans. (2007) 2099.
[27] M.I. Kolinko, I.V. Kityk, A.S. Krochuk, J. Phys. Chem. Solids 53 (10) (October 1992) 1315–1320.
[28] F. Tran, P. Blaha, Phys. Rev. Lett. 102 (2009) 226401.
[29] A.H. Reshak, Phys. Chem. Chem. Phys. 16 (2014) 10558.
[30] G.E. Davydyuk, O.Y. Khyzhun, A.H. Reshak, H. Kamarudin, G.L. Myronchuk, S.P. Danylchuk, A.O. Fedorchuk, L.V. Piskach, M. Yu Mozolyuk, O.V. Parasyuk, Phys. Chem. Chem. Phys. 15 (2013) 6965.
[31] A.H. Reshak, Y.M. Kogut, A.O. Fedorchuk, O.V. Zamuruyeva, G.L. Myronchuk, O.V. Parasyuk, H. Kamarudin, S. Auluck, K.J. Plucinskig, Jiri Bila, Phys. Chem. Chem. Phys. 15 (2013) 18979.
[32] Ali H. Reshak, D. Stys, S. Auluck, I.V. Kityk, Phys. Chem. Chem. Phys. 13 (2011) 2945.
[33] P. Villars, L.D. Calvert (Eds.), Pearson's Handbook of Crystallographic Data for Intermetallic Phases, second ed., ASM International, Materials Park, OH, 1991. P. Villars, Pearson's Handbook of Crystallographic Data for Intermetallic Phases, ASM International, Materials Park, OH, desktop edn., 1997.
[34] ICSD Database, Fachinformationszentrum, 2008. Karlsruhe, Germany.
[35] P. Blaha, K. Schwarz, G.K.H. Madsen, D. Kvasnicka, J. Luitz, An Augmented Plane Wave Plus Local Orbitals Program for Calculating Crystal Properties, WIEN2k, Vienna University of Technology, Austria, 2001.
[36] J.P. Perdew, S. Burke, M. Ernzerhof, Phys. Rev. Lett. 77 (1996) 3865.
[37] F. Bassani, G.P. Parravicini, Electronic States and Optical Transitions in Solids, Pergamon Press Ltd., Oxford, 1975, pp. p149–154.
[38] Fang Wu, Hong zhang Song, Jian feng Jia, Xing Hu, Prog. Nat. Sci. Mater. Int. 23 (4) (2013) 408–412.
[39] F. Wooten, Optical Properties of Solids, Academic press, New York and London, 1972.
[40] D.R. Penn, Phys. Rev. B 128 (1962) 2093.
[41] M. Fox, Optical Properties of Solids, Oxford University Press, 2001.